Exploring the Modification in Physical, Structural and Optical Properties of BaO-PbO-B₂O₃ Glasses by Incorporating Sm₂O₃

J. Singh^a, G.P. Singh^{a,*}, P. Kaur^a, T. Singh^a, I. Singh^a, S. Kaur^b, I. Singh^c and D.P. Singh^b

^aP.G. Department of Physics, Khalsa College, Amritsar 143002, India

Received: 16.07.2025 & Accepted: 11.09.2025

Doi: 10.12693/APhysPolA.148.124 *e-mail: gp_physics96@yahoo.co.in

Using the melt-quench technique, barium-lead borate glasses have been successfully manufactured with various concentrations of samarium ion, and the optical and physical characteristics of the system have been studied. Physical properties like density (ρ) , molar volume (V_m) , average boron-boron separation (d_{B-B}) , polaron radius (r_p) , inter-nuclear distance (r_i) , field strength (F), and oxygen packing density (OPD) are calculated. In addition, using the absorption spectra of the studied glasses, the optical bandgap values have been computed from Tauc's plot and observed to decrease from 3.41 to 3.22 eV with increasing samarium concentration. Furthermore, with increasing Sm concentration, the boronboron separation (d_{B-B}) is seen to decrease, while the OPD increases. In fact, the increasing density and molar weight of the glasses are due to substituting lower molar mass boron with higher molar mass samarium. The introduction of Sm₂O₃ as a modifying oxide causes the density of the glasses to increase. Fourier-transform infrared and X-ray diffraction measurements confirm the amorphous character of the matrix, as well as the presence of several functional groups. The influence of Sm₂O₃ concentration on the host glass is investigated by calculating and considering all physical parameters. In luminescence experiments, the reddish-orange region of the sample with 1 $\hat{\text{mol}}$ % of $\hat{\text{Sm}}^{3+}$ was the most intense. Colorimetric variables, such as CIE coordinates, are also measured. The data show that the studied glasses are appropriate for yellowish-orange to reddish-orange luminescence devices and visible lasers.

topics: samarium oxide, CIE, optical absorption, physical properties

1. Introduction

Researchers have recently become very interested in the development of optical materials with embedded transition metals and rare earth (RE) ions, due to many applications of these materials in solid-state lighting [1, 2], optical memories [3], fiber-optic communications [4–6], laser applications [7], display devices, etc. [8–14]. In recent years, the creation of cutting-edge electronic equipment has increasingly relied on materials with outstanding dielectric characteristics and adaptable architectures [15, 16].

Among many other materials, glasses have attracted a lot of interest from the technical and scientific world due to their special and unique physical, mechanical, and chemical properties [17, 18]. What distinguishes glass from other materials, and which results from its non-porous structure, is its superior chemical stability, insulation from electricity,

and practical mechanical features, as well as lower charge leakage and dielectric losses [19, 20]. Additionally, it was discovered that glasses doped with ions, especially rare earth ions, have some advantages over other materials, such as phosphors [10]. The glass is simple to manufacture, and ions from rare earth elements dissolve well in it [21]. For over a decade, rare earths (RE)-doped glasses have gained considerable interest due to their optical, physical, and chemical properties [22–25].

Borate-based glasses are the most often utilized glass network types across various glass systems. They have a distinctive blend of optical, physical, and chemical characteristics that make them ideal for a variety of technological applications, including optoelectronics and electricity [26]. The creation of new glass materials for technology is motivated by the technological uses of these glass products. Rare earth ion-doped glasses have large spectral regions that span from the ultraviolet to

^bDepartment of Physics, Guru Nanak Dev University, Amritsar 143005, India

^cDepartment of Physics, Akal University, Talwandi Sabo 151302, India

the infrared [27, 28]. The electronic structure of the rare earth ions in rare earth ion-doped glasses, which has a significant influence on the laser properties of these glasses, depends on the compositions of the host glass [27]. A small amount of RE^{3+} ions can be added to the glass to increase its mechanical, physical, and chemical stability characteristics, making it more suitable for advanced applications [29–31]. It is clear from the literature that each rare earth ion has distinct properties because of its electronic transitions 4f-4f and 4f-5d [32]. These ions include Dy^{3+} , Sm^{3+} , Eu^{3+} , Yb^{3+} , Nd^{3+} , and $\mathrm{Er^{3+}}\text{-doped}$ materials for lasers, white lightemitting diodes (W-LED), optical fibers, and applications in tunable lasers. These advantages make it feasible to create optoelectronic devices such as lasers, light converters, solid-state lightning devices, and optical amplifiers that base their operation on the RE ion emission regions when glass networks containing RE ions are used.

Samarium ions (Sm^{3+}) are trivalent lanthanide ions that have a high atomic number, a large ionic radius, and are very resistant to humidity, which has a major influence on the optical and structural characteristics of glasses [32, 33]. Potential uses for Sm_2O_3 -doped amorphous materials include solid-state lasers, electronic devices, color displays, and high-density optical storage systems [34, 35]. Improved fluorescence from the ultraviolet to visible range is displayed in glasses doped with samarium (Sm^{3+}) ions, making them useful in underwater communication, medical diagnostics, color displays, and other applications [36, 37].

These factors have led to several studies documenting the various uses of Sm in various glasses. For example, the TeO₂-BaO-Li₂O-GeO₂:Sm₂O₃ system was studied by Ataullah et al. [38], who concluded that this glass system is favorable for diodes that emit orange light. Additionally, the process of energy transfers in a zinc strontium fluoroborosilicate (ZSFBSi) glass system containing Sm⁺³ was described by Ravina et al. [39]. Additionally, G. Neelima et al. [40] looked into the potential applications of oxyfluorophosphate glasses containing Sm³⁺ ions in displays and lasers. The role of the CIELab diagram in deciphering the process of emission of boro-tellurite glasses loaded with samarium ions (Sm³⁺) for use in optoelectronic devices was examined by S. Ghosh et al. [41]. The impact of samarium oxide on the ligand field parameters and the structural characteristics of iron cations within sodium borate glass was investigated by M.S. Sadeq et al. [42]. As for visible laser and radiation protection applications, G. Dedeepya et al. [43] investigated the optical response features and radiation protection capabilities of tungsten alkali borate glasses activated with Sm³⁺ ions. Spectroscopic evaluations of phospho-borate glasses doped with Sm³⁺ ions in combination with fluoride modifiers were performed by A. Indhrapriyadarshini et al. [44] for applications in the reddish-orange visible light range. The effect of Sm₂O₃ on the optical, structural, thermal, and electrical features of LiBaBO₃ glasses was examined by B.A. Kumar and his coworkers [45]. The radioluminescence and photoluminescence (PL) characteristics of a Sm³⁺-doped Gd–Ba–Na borate glass scintillator were examined by N. Luewarasirikul et al. [46].

Adding more oxides to glass compositions can result in significant improvements in a number of glass properties. The introduction of lead oxide (PbO) - the most efficient modifier added to the glass network [47] — results in the development of BO₃ and BO₄ units with non-bridging oxygen (NBO) groups [48], improves the stability of glass formation, and increases the chemical durability of the materials that are produced [49]. When compared to other modifiers, it provides the best density and absorption of γ -radiation. PbO-containing glass systems provide improved defence against γ and X-ray radiation [47]. Because of great radiation-blocking capabilities, PbO glasses are employed to create windows, walls, and doors in radiotherapy centers, radiation research laboratories, and nuclear power plants [50]. BaO is another interesting alkaline earth metal that may be included in a glass system to enhance its various features [50, 51] and is a frequently used oxide glass modifier that makes the glass material more flexible and less brittle [52]. BaO enhances thermal characteristics when included in a glass system [52]. By reducing the manufacturing temperature and avoiding glass clustering and crystallization, glass modifiers such as BaO can enhance the glass matrix and overcome certain limitations [53]. The optical bandgap of glasses decreases as BaO is added in larger amounts. Furthermore, BaO efficiently occupies voids and prevents cracks by filling the interstitial sites within the glass network [54]. It has superior shielding features, which are advantageous for applications involving radiation protection [55]. When compared to various glass modifiers, BaO has a lower cutoff in the ultraviolet (UV) range, which makes it very useful in optical applications. This unique property makes it possible for glasses made of BaO to transmit UV light more efficiently. As a result, these glasses are perfect for uses where effective UV light transmission is essential, such as lasers and solar cells [56].

Similarly, in recent decades, plenty of reports have been published on structural investigations and other aspects of glasses containing ${\rm Sm}^{3+}$ ions. However, ${\rm Sm}^{3+}$ -doped barium—lead borate glasses have not been thoroughly studied. Given the numerous scientific arguments provided regarding the previously mentioned chemical components, we created multi-component ternary glasses containing borate and doped with samarium ions. The objective of the current investigation is to understand how ${\rm Sm}_2{\rm O}_3$ impacts many properties, including structural, optical, physical, and luminescent ones, and therefore to determine the practical applications these glasses may have in optoelectronic devices.

2. Materials and methods

2.1. Preparation of glasses

Using the melt-quenching process, a series of glass samples with the formula $x\operatorname{Sm}_2\operatorname{O}_3$ -(20-x) BaO-20PbO-60B₂O₃ and $0 \le x \le 2 \text{ mol}\%$ were formed. After being ground into a fine powder, the necessary mixture of chemicals — lead oxide (PbO) (99% purity), samarium oxide (Sm_2O_3) (99.9% purity), barium oxide (BaO) (99.9% purity), and boric oxide (B_2O_3) (99.5% purity) — is melted in a silicon crucible at 1200°C for 60 min until a uniform liquid devoid of bubbles forms. To ensure that the sample won't break due to any remaining internal strains, the melt is poured into a preheated steel mold that has been and then annealed for 1 h at 440°C. The resulting samples are polished with cerium oxide to achieve the highest level of flatness [57]. Table I provides the nominal composition of the prepared glasses. The physical appearance of glasses is shown in Fig. 1.

2.2. Experimental methods

X-ray diffraction (XRD) analysis utilizing a PAN-alytical X'Pert PRO X-ray diffractometer at a scanning rate of $4^{\circ}/\text{min}$ with 2θ changed in the range of $10^{\circ}-70^{\circ}$ confirms the samples' amorphous/crystalline nature.

A Fourier transform computerized infrared spectrometer (IRAffinity-1 Shimadzu spectrometer type) is used to measure the glasses' infrared transmission spectra at room temperature, with wave numbers in the range of $400-4000~\rm cm^{-1}$. Glass powder and KBr are combined in a 1:100 ratio to create a fine powder from the prepared glasses. To create uniform pellets, the weighed mixtures are subsequently compressed to $150~\rm kg/cm^2$. The infrared transmission measurements are taken immediately after the pellets are prepared.

A sensitive microbalance using pure benzene as immersion fluid is utilized to estimate the room temperature density of glass samples using the standard Archimedes' principle.

The density is then calculated using

$$\rho = \frac{W_a}{W_a - W_b} \rho_b,\tag{1}$$

where W_a is the weight of the sample in air, W_b is the weight of the sample in benzene, and ρ_b is the density of benzene.

A UV-Visible spectrophotometer (Shimadzu, Japan) is used to record the optical absorption spectra of samples in the 200–1100 nm range at room temperature.

The photoluminescence analysis of the glasses is conducted using a Perkin Elmer LS 45 spectrometer at an excitation wavelength of 402 nm.



Fig. 1. Physical appearance of prepared glasses.

TABLE I

Chemical composition [mol%] of the prepared glass samples.

Sample	$\mathrm{Sm_2O_3}$	BaO	PbO	$\mathrm{B}_{2}\mathrm{O}_{3}$
$\mathrm{Sm}0$	0	20	20	60
$\mathrm{Sm}0.5$	0.5	19.5	20	60
$\mathrm{Sm}1$	1	19	20	60
$\mathrm{Sm}1.5$	1.5	18.5	20	60
$\mathrm{Sm}2$	2	18	20	60

The CIE (Commission Internationale de l'Éclairage, France) color coordinates of the prepared Sm³⁺-doped glasses were calculated from the emission spectra, in the framework of the 1931 CIE chromaticity diagram.

3. Results and discussion

3.1. X-ray diffraction (XRD)

As illustrated in Fig. 2, the X-ray diffraction (XRD) pattern of the glasses was observed at angles ranging from 10° to 70°. The long-range structural disorder in these glasses is indicated by the diffuse scattering seen in the XRD pattern at lower angles [21, 22]. The absence of sharp peaks and the existence of a broad halo can be seen, reflecting the amorphous state of our manufactured glasses.

3.2. Fourier transform infrared (FTIR) spectroscopy analysis

The structural building groups of the glasses under study are reflected in the infrared vibrational peaks. The chemical components, including their percentage and arrangement, determine the structural building units. Four bands between 400 and $1420~{\rm cm}^{-1}$ are visible in the Fourier transform infrared (FTIR) spectra of rare earth (RE) ions present in borate glasses.

(i) The vibrations of metal cations are responsible for the formation of the band between 400 and 600 cm^{-1} .

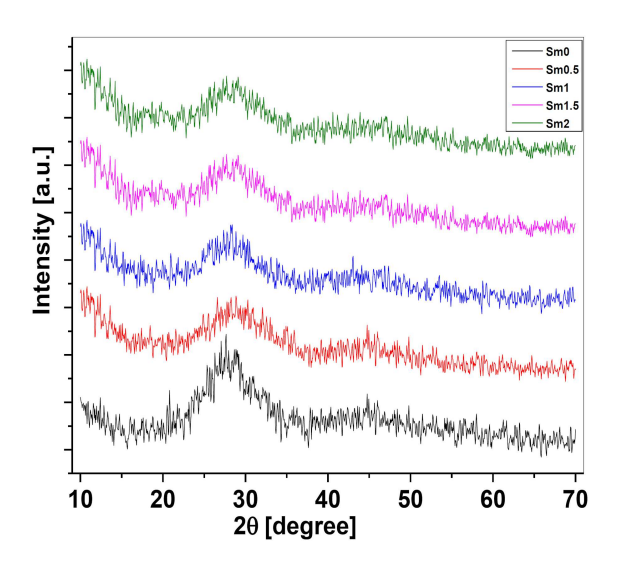


Fig. 2. XRD patterns of prepared glasses.

- (ii) The B–O–B bending vibrations of BO_4 and BO_3 groups are responsible for the formation of the band between 600 and 800 cm⁻¹.
- (iii) The band between 800–1200 cm $^{-1}$ is caused mostly by borate's BO₄ groups.
- (iv) The BO_3 groups are responsible for the formation of the band between 1200 and 1400 cm⁻¹.

Additionally, the water group's O–H vibration is responsible for the band from $2400 \text{ to } 4000 \text{ cm}^{-1}$ [58–62].

It is well-established that borate glass essentially consists of two structural units, namely BO_3 and BO_4 units [32, 33, 63]. By adding the modifier oxides, a strong conversion between them can occur. As shown in Fig. 3, the spectra of FTIR for samarium-doped and undoped glasses are recorded in the $400-4000~\rm cm^{-1}$ range at room temperature.

The band centered at $709~\rm cm^{-1}$ in the sample Sm0 (read as 0 mol% of samarium) is identified as the bending vibration of the B–O–B bonds of BO₃ and BO₄ groups [64]. The symmetrical stretching vibration of the B–O bonds within units of BO₄ from the tri, tetra, and pentaborate groups is related to the band at 961 cm⁻¹ [64, 65]. The symmetrical stretching vibration of B–O bonds within BO₃ units in metaborate groups is represented by the band at 1346 cm⁻¹ [66].

The location of these bands shifts when the rare earth metal oxide $\rm Sm_2O_3$ is added to the glass system (in samples $\rm Sm0.5-Sm2$). This shift is probably caused by modifications of the structure of glasses, specifically the formation of new bridge bonds with metal ions (Pb⁴⁺) [66, 67].

Additionally, the intensity of the band centered at 954 cm⁻¹ increases when the Sm concentration rises from 0.5 to 2 mol%. This band is associated with tetrahedral BO₄ borate groups [68], as was previously mentioned. When the mole percentage of

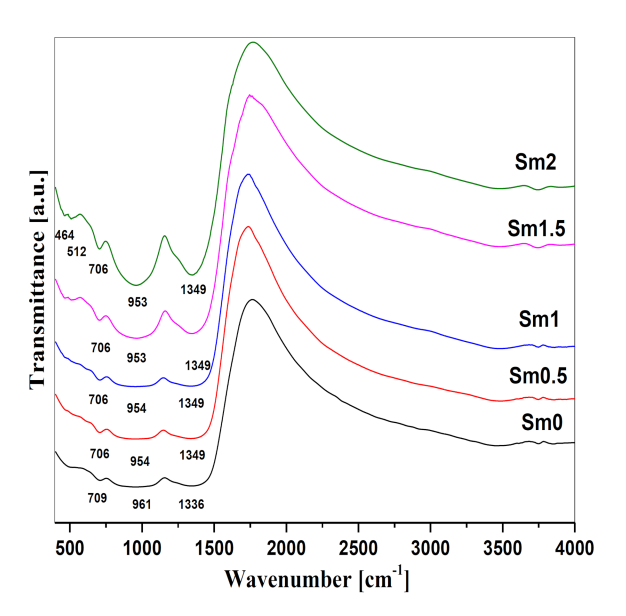


Fig. 3. FTIR spectra of Sm_2O_3 glasses.

samarium in sample Sm2 is 2%, the intensity of this band (at $954~\rm cm^{-1}$) increases to its maximum. This finding indicates that BO₃ groups are converted to BO₄ groups when samarium is present [68, 69]. Additionally, it is noted that a new tiny band in the $410\text{--}550~\rm cm^{-1}$ region appears when the samarium concentration is between 1.5 and 2%. The vibrations of metal cations, particularly those resulting from the presence of bending vibrations of the PbO₄ tetrahedral units, are attributed to these bands [70, 71]. The minor peak seen in the $3500\text{--}4000~\rm cm^{-1}$ region in all glasses is attributed to the basic stretching of the water or hydroxyl groups.

In order to get more precise information about the structural groups in the samples, the experimentally observed bands are subjected to deconvolution. Figure 4 illustrates the results of the deconvolution for sample Sm2 (2 mol% of samarium). From the relative peak areas of BO_3 and BO_4 in structural groups, which are separated by Gaussian deconvolution, the fraction [%] of three- and fourfold coordinated boron is estimated, respectively, as follows [72]

$$N_{\rm BO_3} = \frac{A_3}{A_3 + A_4} \times 100 \tag{2}$$

and

$$N_{\rm BO_4} = \frac{A_3}{A_3 + A_4} \times 100,\tag{3}$$

where A_3 is the area of BO₃ units, calculated in the range 1200–1600 cm⁻¹, and A₄ denotes the area of BO₄ units, calculated in the range 800–1200 cm⁻¹.

Generally, the relative area of a given band can reflect the quantity of structural groups associated with that band, so the relative change of the area of BO_3 and BO_4 groups can be associated with the $BO_3 \rightarrow BO_4$ transformation in the glass network.

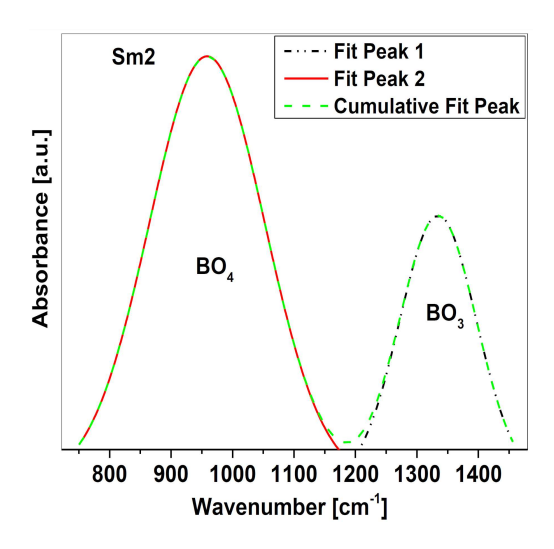


Fig. 4. Deconvolution of FTIR spectra of $\mathrm{Sm2}$ sample.

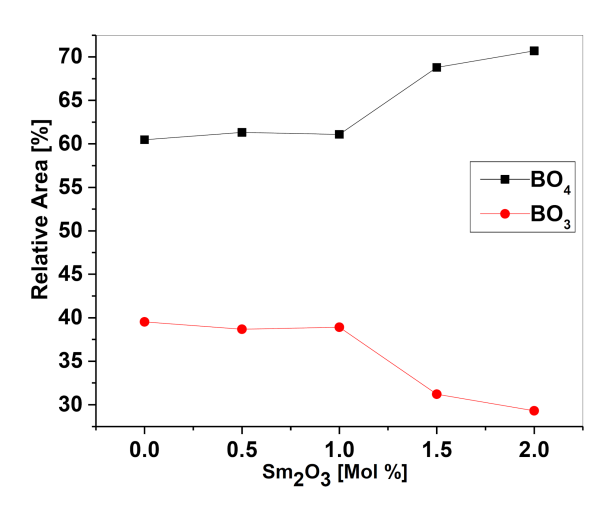


Fig. 5. Dependence of the fraction of BO_3 and BO_4 units on mol% of Sm_2O_3 samples.

It is found that with increasing Sm_2O_3 content, the BO_4 units content increases, which signifies the modifier function of Sm_2O_3 . The dependence of the N_{BO_4} and N_{BO_3} ratio on samarium content is shown in Fig. 5. It is observed that the content of N_{BO_4} units increases and that of N_{BO_3} decreases with increasing Sm_2O_3 concentration, revealing the transformation of BO_3 to BO_4 units. It is clearly seen in Fig. 4 that a larger number of BO_4 groups is formed at higher concentration of samarium (1.5 and 2 mol%) in the glass network.

3.3. Physical properties of glasses

A number of physical parameters indicated in Table II can be used to verify the compactness of the glass structure. As the mole concentration of samarium oxide in the manufactured glass samples

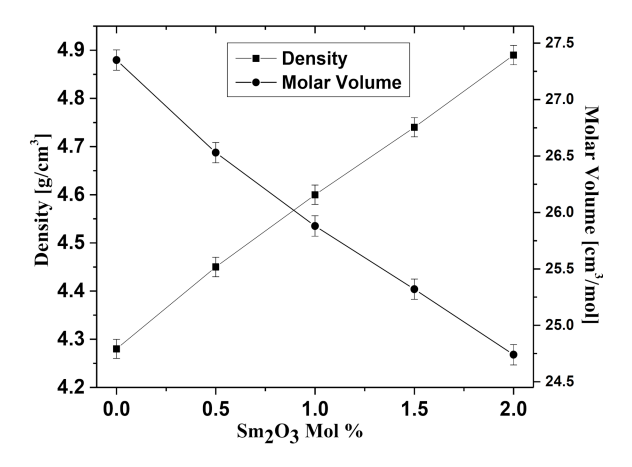


Fig. 6. Variation of density and molar volume with mol% of $\mathrm{Sm_2O_3}$ of glasses with error bars.

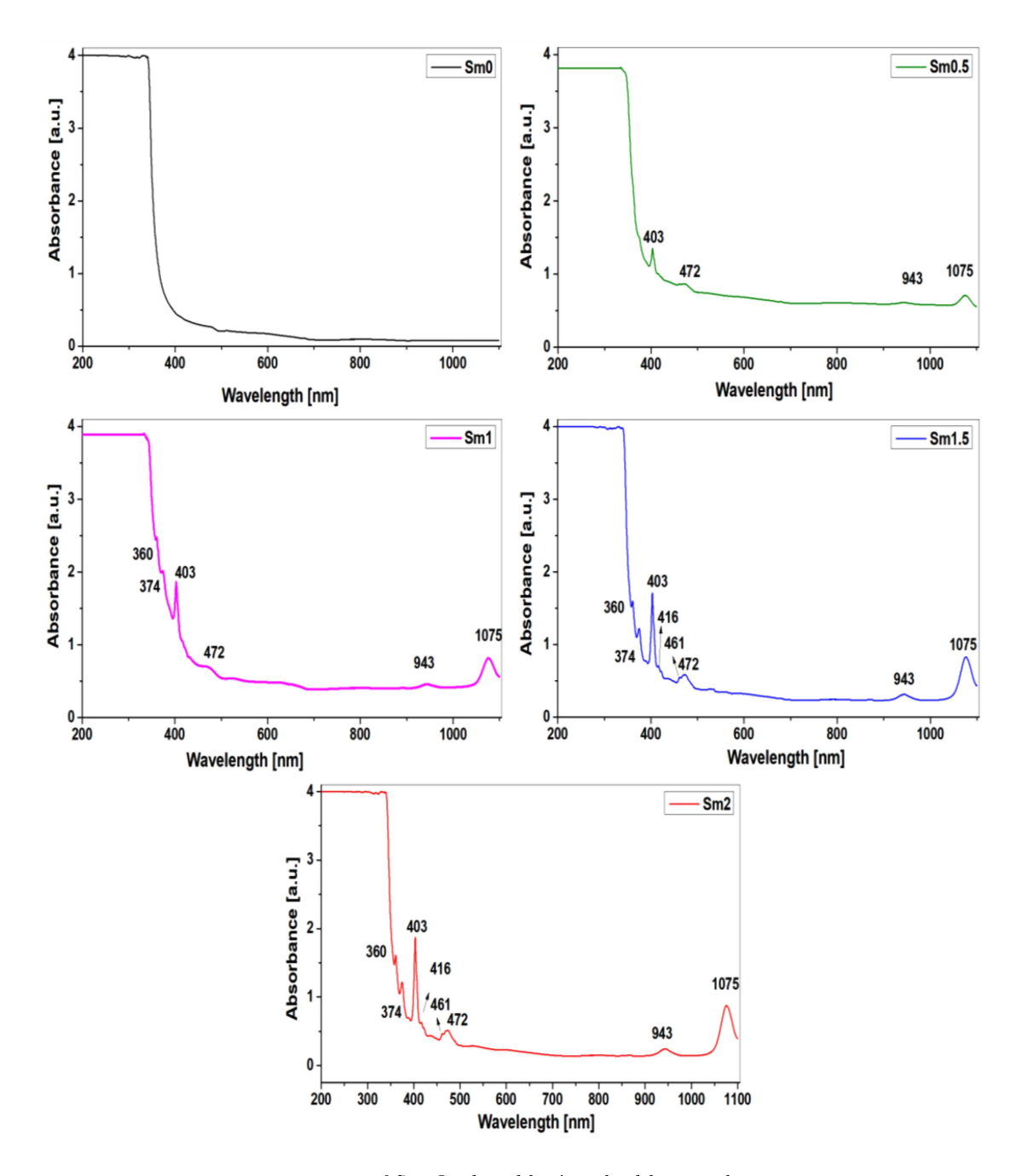
increases, the density (ρ) of glass increases correspondingly. As the amount of samarium oxide grows from 0 to 2 mol\%, density values rises from 4.28 to 4.89 g/cm³. The sample with the highest samarium content is the one having the highest density. Additionally, it has been noted that as Sm-concentration is higher, the molecular weight of glasses increases steadily [73]. The substitution of higher molar mass samarium for lower molar mass boron is the cause of this increase in density and molar weight [74]. The transformation of trigonal BO₃ groups into tetrahedral BO₄ groups is another factor [75, 76]. Tetrahedral BO₄ groups, which are more stable, form a compact glass structure [77]. This increase in density indicates that the samarium addition contributes to the glass system's improved packing density [77]. Additionally, the molar volume (V_m) values obtained are the inverse of the density results, meaning that as the Sm₂O₃ content increases, molar volume value falls. These results validate the glass structure's shrinking.

Figure 6 illustrates the relationship between density (ρ) and the molar volume (V_m) of the resulting glass and how they alter when Sm_2O_3 is added. The oxygen packing density, average boron-boron separation (d_{B-B}) , polaron radius (r_p) , average rare earth ion concentrations (N), inter-nuclear distance (r_i) , and field strength (F) of the Sm-O bond of samarium have also been calculated using standard formulae and are listed in Table II. By assessing the characteristics such as polaron radius (r_p) , average boron-boron separation (d_{B-B}) , inter-nuclear distance (r_i) , field strength (F), and oxygen packing density (OPD), it is also possible to verify the rigidity of glasses [74, 75, 78]. The value of V_{mb} , which is connected to the ionic radii of boron, determines the cation ratio within the glass matrix in the typical boron-boron separation. Additionally, the boronboron separation was shortened as a result of the addition of Sm_2O_3 to the glass structure [74, 78].

Physical and optical parameters of the prepared glass samples.

TABLE II

Sample	Density $[g/cm^3]$ ± 0.02	$\begin{array}{c} \text{Molar} \\ \text{volume} \\ [\text{cm}^3/\text{mol}] \\ \pm 0.09 \end{array}$	Boron-boron separation $(d_{\mathrm{B-B}})$ [nm]	$\begin{array}{c} {\rm OPD} \\ {\rm [mol/cm^3]} \end{array}$	RE ions concentration (N)	Polaron radius (r_p) [Å]	$egin{array}{c} ext{Inter-} \ ext{nuclear} \ ext{distance} \ (r_i) ext{[Å]} \end{array}$	Field strength $(\times 10^{17})$	Band gap [eV]
$\mathrm{Sm}0$	4.28	27.35	0.384	80.43	0	_	_	_	3.41
$\mathrm{Sm}0.5$	4.45	26.53	0.380	83.31	1.14	1.79	4.45	1.93	3.34
Sm1	4.60	25.88	0.377	85.79	2.33	1.41	3.505	3.11	3.26
$\mathrm{Sm}1.5$	4.74	25.32	0.376	88.08	3.57	1.22	3.038	4.14	3.24
$\mathrm{Sm}2$	4.89	24.74	0.372	90.54	4.87	1.10	2.74	5.09	3.22



 $\label{eq:continuous} Fig.~7.~~UV\mbox{-}visible~absorption~spectra~of} ~Sm_2O_3\mbox{-}doped~barium\mbox{-}lead~borate~glasses.$

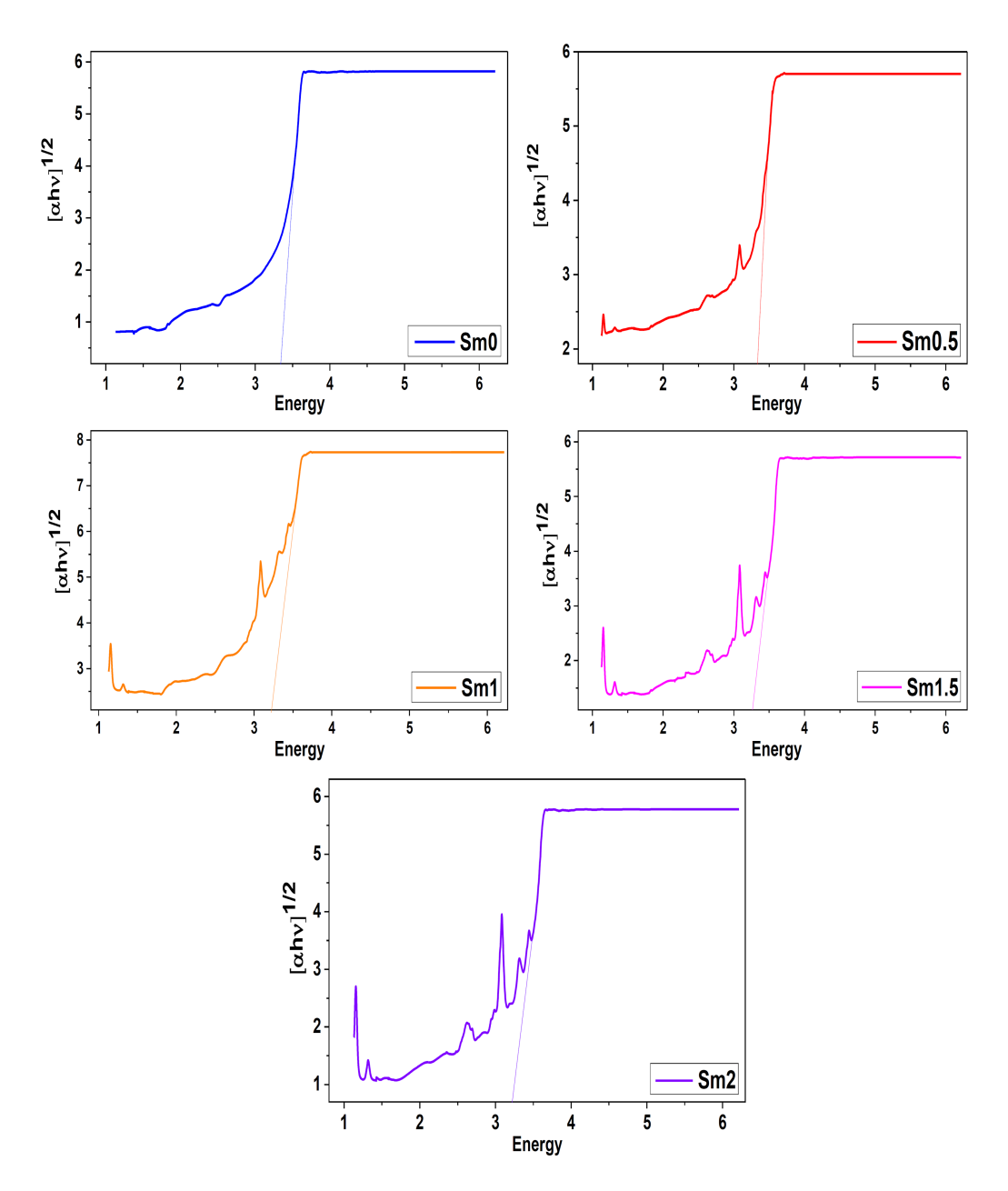


Fig. 8. Tauc plot of the prepared glasses.

The polaron radius (r_p) and inter-nuclear distance (r_i) are also showing a downward trend [79], which supports this conclusion. The polaron radius, which decreases as the dopant concentration increases, can be used to diagnose the interactions between ions and the glassy matrix [73]. A decline in the distance between a doped element's cation and anion is indicated by the glasses' shorter inter-nuclear distance as the Sm_2O_3 content increases [74]. The glass network thus gets more compact and exhibits outcomes that are consistent with the density data. Stronger bonding strengthens the field strength (F)surrounding the samarium ion and makes the glass network more compact [75, 80]. As Sm₂O₃ content increases, the glasses' OPD keeps rising, i.e., the inclusion of samarium increases the rigidity of oxygen packing in a prepared glass network. With the addition of samarium ions, all of these results for various parameters support a compact glass structure.

3.4. Optical properties

The UV-Visible (UV-Vis) optical absorption spectra of all prepared Sm^{3+} -doped barium—lead borate glasses, recorded at room temperature, are demonstrated in Fig. 7. These spectra have a number of inhomogeneously broadened bands with varying intensities. Typical f-f transitions from the ground state of Sm^{3+} ions to their different excited states are represented by these bands. The starting

point for all transitions is the ground state of samarium, which is the initial level ${}^6H_{5/2}$ [81, 82]. Due to the transitions from the ground level ${}^6H_{5/2}$ to numerous excited $^{2s+1}L_J$ levels, absorption peaks appear, and most of these transitions are electric dipole in nature, according to the selection rule $\Delta J \leq 6$. Some transitions have a magnetic dipolar nature with the selection rule $\Delta J = 0, 1$, such as the ${}^6H_{5/2} \rightarrow {}^4G_{5/2}$ transition around 560 nm it is not present in our case [81, 82] because it is highly sensitive to the local environment surrounding the samarium ions in the glass matrix. The transition at about 403 nm (or ${}^6H_{5/2} \rightarrow {}^6P_{3/2}$) is the most intense because it is an exception to the spin prohibition that governs all transitions in the UV and visible spectral region [83, 84]. The optical absorption spectra of the glasses change significantly when Sm_2O_3 is added to the sample Sm0.5 at the expense of BaO, while the amount of PbO and B₂O₃ remains constant. Samarium (0.5 mol%) in glasses shows four discrete bands at 403, 472, 943, and 1075 nm, which correspond to the samarium transitions ${}^6H_{5/2} \rightarrow {}^6P_{3/2}$, ${}^4M_{15/2}$, ${}^4I_{11/2}$, and ${}^6F_{11/2}$, respectively [83–86]. These peaks are absent in the sample Sm0 (sample without samarium). All absorption bands have very low intensity in the sample Sm0.5. In the sample Sm1 (i.e., at 1 mol\% of Sm), two additional bands appear at 360 and 374 nm, which correspond to the transitions ${}^{6}H_{5/2} \rightarrow {}^{4}D_{3/2}$ and $^6H_{5/2} \rightarrow ^6P_{7/2}$, respectively [81, 85]. Also, these band intensities increase in the sample Sm1 with increasing samarium content. At 1.5 mol% of samarium (in the sample Sm1.5), in addition to these bands, one weaker peak at 416 nm is seen, which is absent in the samples Sm0.5 and Sm1. This peak is due to the transition $^6H_{5/2} \rightarrow ^6P_{5/2}$ [81, 85]. As the concentration of samarium increases further (to 2%), it turns out that Sm helps to boost the peak intensity — in the absorption spectra the intensity of all peaks rises, even if the lead and borate concentration maintain constant. Therefore, it may be inferred that samarium inclusion causes the optical changes in the glass network. The amorphous nature of the glass causes the absorption bands to be so broad [87].

3.5. Optical band gap (E_{opt})

Now we can calculate the indirect optical band gap for the glasses we studied using the following equation provided by Tauc [88]

$$(\alpha h\nu)^{1/2} = B\left(h\nu - E_{opt}\right),\tag{4}$$

where α denotes the absorption coefficient close to the band edge, $h\nu$ corresponds to the incident energy radiation, and B denotes the band tailing parameter. The optical band gap of the glasses under examination was determined using a plot of $(\alpha h\nu)^{1/2}$ and $h\nu$, as illustrated in Fig. 8.

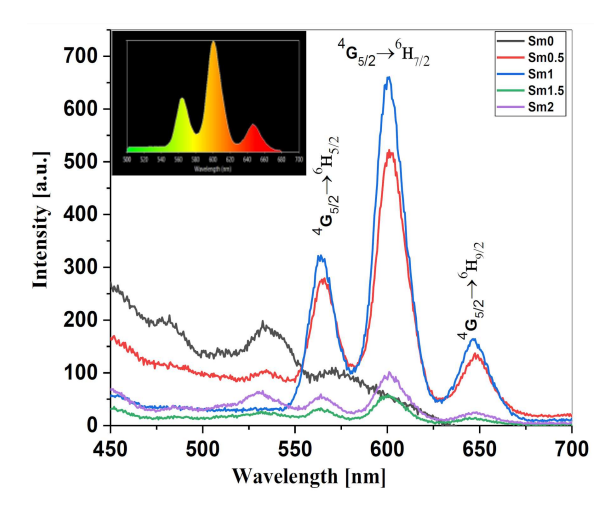


Fig. 9. Emission spectra of glasses recorded at 402 nm excitation with embedded colored representation of PL emission of sample Sm1.

Here, the optical band gap values E_{opt} follow the trend Sm0 > Sm0.5 > Sm1 > Sm1.5 > Sm2, with corresponding values of 3.41, 3.34, 3.26, 3.24, and 3.22 eV.

The higher concentration of BO_4 units in the Sm2 sample, which causes the network to become denser and the band gap to narrow, may explain why the band gap has its minimum value. In comparison to the other compositions obtained in this study, the density data for Sm2 glass show a compact structure, which is consistent with the band gap values.

3.6. Photoluminescence (PL) spectroscopy

Figure 9 displays the emission spectra of Sm³⁺doped BaO-PbO-B₂O₃ glasses at various samarium ion concentrations at an excitation wavelength of 402 nm, which corresponds to $({}^6H_{5/2} \rightarrow {}^6P_{3/2})$. Because of the f-f transitions in the Sm³⁺ (4 f_5) structure, the created glass samples exhibit intense visible emission in the orange—red region. The three notable emission bands in these series' emission spectra, which correspond to the ${}^4G_{5/2}
ightarrow {}^6H_J$ transition (for J = 5/2, 7/2, 9/2) at 564, 602, and 642 nm, respectively, are transitions from the common ${}^4G_{5/2}$ level to low-lying levels. These bands have an intensity order of ${}^4G_{5/2} \rightarrow {}^6H_{7/2} \gg$ $^6H_{5/2} \gg ^6H_{9/2}$, and follow the same pattern in all analyzed samples. As the concentration of Sm₂O₃ increases, there is no band shift. Broad bands in the $500\text{--}600~\mathrm{nm}$ range are also seen at $534~\mathrm{and}~571~\mathrm{nm}$ in pure samples. Large accumulation of Pb²⁺ ions $({}^{3}P_{1} \rightarrow {}^{1}S_{0})$ and Sm^{3+} $({}^{4}F_{3/2} \rightarrow {}^{6}H_{5/2})$ ion emission may be responsible for these bands [89, 90]. As the emission intensity of Sm³⁺ ions increases, the intensity of these bands noticeably decreases.

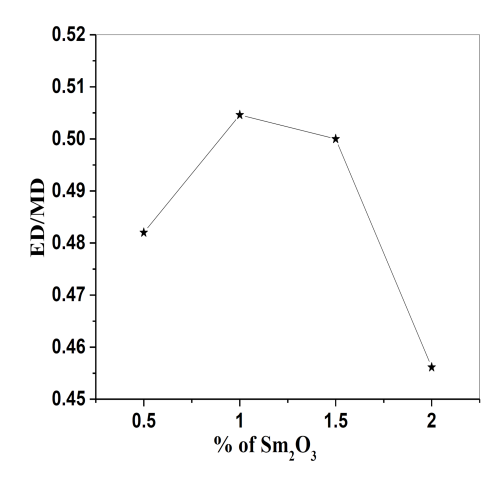


Fig. 10. Variation of ED/MD with Sm₂O₃.

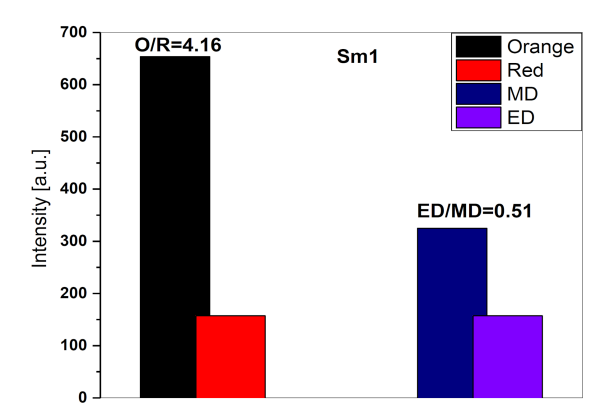


Fig. 11. $\mathrm{O/R}$ and $\mathrm{ED/MD}$ parameter ratios of sample Sm1.

While the transition ${}^4G_{5/2} \to {}^6H_{9/2}$ is purely electric dipole allowed with the selection rule $\Delta J=2$, the transition ${}^4G_{5/2} \rightarrow {}^6H_{5/2}$ is magnetic dipole allowed with $\Delta J=0$. In contrast, the transition ${}^4G_{5/2} \rightarrow {}^6H_{7/2}$ is electric dipole dominant but allows magnetic dipoles with the selection rule $\Delta J = \pm 1$. As the samarium concentration rises, the fluorescence intensity of these transitions increases as well, peaking at 1 mol%. A sudden drop in luminescence intensity, leading to luminescence quenching, occurs at a concentration of $\simeq 1.5 \text{ mol}\%$ samarium. The distances between rare earth ions would be shortened with an increase in Sm³⁺ ions, leading to improved dipole-quadrupole interactions between Sm³⁺ ions, because high concentrations result in the formation of clusters of Sm³⁺ ions through Sm-O-Sm bonds. Non-radiative transitions are produced when the excitation energy is transferred from one stimulated luminescent center in the cluster to another by cross-relaxation or phonon interaction as a result of the interactional agglomeration of nearby rare earth ions of Sm³⁺ ions [73, 91]. In this glass system, the ideal Sm³⁺ concentration is roughly 1 mol%.

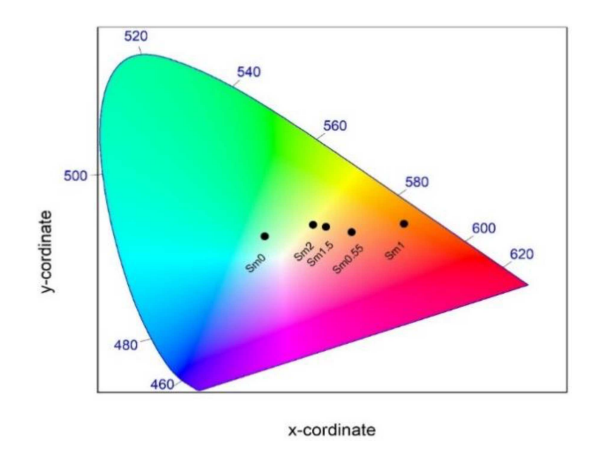


Fig. 12. CIE chromaticity diagram showing the emission color under excitation of 402 nm for prepared glass systems.

 $\begin{tabular}{ll} TABLE\ III\\ CIE\ 1931\ chromaticity\ coordinates\ of\ prepared\ glass\\ systems. \end{tabular}$

Sample	Color coordinates			
Sample	x coordinate	y coordinate		
$\mathrm{Sm}0$	0.38	0.28		
$\mathrm{Sm}0.5$	0.40	0.43		
$\mathrm{Sm}1$	0.42	0.52		
$\mathrm{Sm}1.5$	0.41	0.39		
$\mathrm{Sm}2$	0.41	0.37		

The local environment of the host matrix exhibits a high degree of sensitivity to the electric dipole (ED) transition. The ratio between ${}^4G_{5/2} \rightarrow {}^6H_{9/2}$ (ED) and ${}^4G_{5/2} \rightarrow {}^6H_{5/2}$ (MD — the magnetic dipole) transitions is known as the asymmetric ratio (R) or luminescence intensity ratio and is used to analyze the asymmetry around the Sm³⁺ ion site. The environment is symmetric or depends on the intensity of the ED transition [92], i.e., the glass matrix with a larger intensity of the electric dipole transition indicates a more asymmetric nature around the RE³⁺ ions. In the present study of glasses, the spectral intensity of the ${}^4G_{5/2} \rightarrow {}^6H_{5/2}$ (MD) transition is larger than the intensity of the ${}^4G_{5/2} \rightarrow {}^6H_{9/2}$ (ED) transition, indicating the symmetric nature of the host glass. The ED/MD parameter for the Sm0.5, Sm1, Sm1.5, and Sm2 samples are 0.481, 0.505, 0.5, and 0.456, respectively. The ED/MD variations of prepared samples are shown in Fig. 10. These results indicate that the sample Sm1 has a higher value of ED/MD, i.e., lower symmetry than other samples, which might be due to a decrease in covalency of the ligand field around the Sm^{3+} ion site.

For further analysis, the intensity of the orange band (${}^4G_{5/2} \rightarrow {}^6H_{7/2}$) was compared to the intensity of the red band (${}^4G_{5/2} \rightarrow {}^6H_{9/2}$). The

values of the orange-to-red (O/R) ratio are found to be 4.20, 4.16, 4.09, and 4.50 for the Sm0.5, Sm1, Sm1.5, and Sm2 glasses, respectively. The magnitude of the R/O ratio indicates higher symmetry around the Sm $^{3+}$ ions in the present ligand field. Figure 11 shows the O/R and ED/MD parameter ratios of the Sm1 sample. These variations reveal that the environment around RE ions is modified by reorientation of atoms to new positions, which is also confirmed by FTIR, density, and UV results.

3.7. CIE diagram

The CIE (Commission Internationale de l'Éclairage) 1931 x-y chromaticity diagrams are presented in Fig. 12 for prepared glasses, and the computed color coordinates are listed in Table III. It demonstrates how altering the host matrix composition can affect the luminescence color from yellowish orange to reddish orange to deep red. The quenching of luminescence intensity has also been shown to cause an evident change in color hue.

4. Conclusions

The structural, physical, and spectroscopic characteristics of Sm³⁺ ions in barium-lead borate glasses were investigated using XRD, FTIR, UV-Vis absorption, and luminescence measurements. All manufactured glasses were found to be amorphous by XRD spectra. The influence of Sm₂O₃ on structural changes in the glass network is confirmed by all common physical characteristics. Inside the glasses, the presence of BO₃ and BO₄ functional groups was identified by the FTIR spectra. As the Sm_2O_3 concentration increased from 0 to 2 mol%, the densities of the glasses rose from 4.28 to 4.89 g/cm³. According to the UV-Vis spectra, the presence of samarium caused the optical alteration in the glass network, and the increase in samarium concentration increased the intensity of the bands. Optical bandgap values of the studied glasses were observed to decrease from 3.41 to 3.22 eV with an increase in samarium concentration. Under the excitation wavelength of 402 nm, the photoluminescence spectra of the glasses under study showed orange to reddish-orange to deep-red emission with the most intense band at 601 nm. Energy transfer between Sm³⁺ ions was responsible for the strong emission recorded at 1 mol% Sm₂O₃ concentration and beyond concentration quenching. The Sm1 glass sample's strong emission, which was visible in the deepred area of the CIE diagram, demonstrated its sensitiveness to the human eye and suggested that it could be used in display systems.

Acknowledgments

The authors highly acknowledge the financial support in the form of seed money provided by the Principal of Khalsa College, Amritsar-Punjab. The authors are highly thankful to the Departments of Physics and Chemistry, Khalsa College, Amritsar, for providing the instrumental facility (UV-Visible and FTIR spectroscopes).

References

- [1] Y.D. Narad, Y.R. Parauha, S.J. Dhoble, *J. Non-Cryst. Solids* **655**, 123446 (2025).
- [2] K.O. Brito, O.C. Silva Neto, N.F. Dantas, T.A. Lodi, F. Pedrochi, A. Steimacher, *Opt. Mater.* **165**, 117106 (2025).
- [3] A.M. Ali, A.E. Harby, A.E. Hannora, M.M. El-Desoky, J. Alloys Compds. 1017, 178996 (2025).
- [4] H. Algarni, M.S. Al-Assiri, M. Reben, I.V. Kityk, B. Burtan-Gwizdala, H.H. Hegazy, A. Umar, E. Yousef, R. Lisiecki, Opt. Mat. 83, 257 (2018).
- [5] J. Markiewicz, T. Ragin, P. Miluski, M. Kuwik, G.L.J. Miranda, W.A. Pisarski, J. Pisarska, J. Dorosz, D.Dorosz, M. Kochanowicz, *Ceram. Int.* 51, 16621 (2025).
- [6] K. Kowalska, J. Pisarska, T. Ragiń, J. Markiewicz, M. Kochanowicz, P. Miluski, J. Dorosz, D. Dorosz, W.A. Pisarski, J. Alloys Compds. 1010, 177965 (2025).
- [7] Isha, A. Kumar, Ravina, R. Punia, S. Dahiya, N. Deopa, A. Kumar, *J. Mol. Struct.* 1327, 141203 (2025).
- [8] S.J. Isac, P.V. Kumar, A.P. Dhinakaran, S. Praveenkumar, Opt. Laser Technol. 182, 112111 (2025).
- [9] J. Song, G. Chen, Sustain. Mater. Technol. 43, 01229 (2025).
- [10] I. Khan, M. Shoaib, N.S. Alsaiari, S.M. Wabaidur, G. Rooh, N. Srisittipokakun, I. Ullah, J. Kaewkhao, *Optik* 269, 169821 (2022).
- [11] P.N. Parale, A.R. Kadam, S.J. Dhoble, K.V. Dabre, *Opt. Laser Technol.* 181, 111796 (2025).
- [12] V.R. Teja, M. Sreenivasulu, V.K. Chavan, Ceram. Int. 51, 10077 (2025).
- [13] Z. He, D. Zhou, L. Chen, Y. Ban, Y. Liao, H. Xu, K. Han, Z. Leng, W. Han, Opt. Laser Technol. 183, 112343 (2025).

- [14] A.M. Babu, B.C. Jamalaiah, T. Sasikala, S.A. Saleem, L. RamaMoorthy, J. Alloys Compds. 509, 4743 (2011).
- [15] R.F. Salgueiro, F.E. Maturi, V.M.P. da Silva, D. Manzani, D.S. Carlos, *J. Lumin.* 277, 120932 (2025).
- [16] L.P.R. Kassab, L.F. Freitas, K. Ozga, M.G. Brik, A. Wojciechowski, Opt. Laser Technol. 42, 1340 (2010).
- [17] R.K. Mishra, S.K. Avinashi, S. Kumari, Shweta, R. Nain, T. Katheriya, R.K. Dwivedi, S. Upadhyay, C. Gautam, J. Alloys Compds. 990, 174354 (2024).
- [18] I. Ullah, C.S. Sarumaha, A. Angnanon, I. Khan, M. Shoaib, S.A. Khattak, S. Kothan, N. Sangwaranatee, G. Rooh, J. Kaewkhao, *Ceram. Int.* 49, 13774 (2023).
- [19] D. Biswas, D. Patra, S.B. Hota, A. Das, N. Modak, R. Mondal, S. Kabi, *Phys. B Condens. Matter* **697**, 416728 (2025).
- [20] W. Zheng, T. Liang, Y. Liu, H. Fu, H. Chen, L. Gao, D. Chen, Y. Li, *J. Eur. Ceram. Soc.* 45, 116949 (2025).
- [21] G.P. Singh, P. Kaur, S. Kaur, D.P. Singh, *Phys. B Condens. Matter* **407**, 4168 (2012).
- [22] G.P. Singh, P. Kaur, S. Kaur, D.P. Singh, Phys. B Condens. Matter 407, 4269 (2012).
- [23] X. Li, X. Deng, J. Hong, J. Lin, J. Lv, M. Yu, X. Guan, S. Du, Y. Yu, D. Chen, J. Lumin. 266, 120256 (2024).
- [24] J. Xue, X. Wang, J.H. Jeong, X. Yan, Chem. Eng. J. 383, 123082 (2020).
- [25] A. Madhu, M. Al-Dossari, U.K. Kagola, N.S. Abd EL-Gawaad, C.R. Kesavulu, B. Angadi, N. Srinatha, J. Alloys Compds. 1010, 177583 (2025).
- [26] M.I. Sayyed, C.V. More, S. Biradar, K.A. Mahmoud, *Radiat. Phys. Chem.* 235, 112878 (2025).
- [27] M.G. Moustafa, M.H. Ammar, M. Saad, A. Qasem, E.M. Abdallah, *Opt. Mater.* 141, 113904 (2023).
- [28] M. Nogami, G. Kawamura, G.J. Park, H. You, T. Hayakawa, J. Lumin. 114, 178 (2005).
- [29] D. Rajesh, A. Balakrishna, Y.C. Ratnakaram, *Opt. Mater.* **35**, 108 (2012).
- [30] K. Bansal, S. Kumar, K. Singh, S. Singh, Ceram. Int. 50, 44543 (2024).
- [31] J. Kaur, P. Kaur, I. Mudahar, K. Singh, Ceram. Int. 49, 13610 (2023).
- [32] F. Zaman, J. Abbas, I. Ullah et al., Solid State Sci. 163, 107878 (2025).

- [33] O. Bawazeer, M.S. Sadeq, Radiat. Phys. Chem. 217, 111471 (2024).
- [34] R.N.A. Prasad, L.S. Rao, T.A. Babu, K. Neeraja, N.K. Mohan, *Optik* 244, 167563 (2021).
- [35] I. Khan, M. Shoaib, N. Srisittipokakun, I. Ullah, A. Ahad, S. Kothan, G. Rooh, J. Kaewkhao, Optik 244, 167563 (2022).
- [36] H.M. Elsaghier, A.R. Wassel, M.A. Hassan, S.Y. Marzouk, A. Samir, *Mater. Res. Bull.* 173, 112700 (2024).
- [37] V. Venkatramu, P. Babu, C.K. Jayasankar, T. Tröster, W. Sievers, G. Wortmann, Opt. Mater. 29, 1429 (2007).
- [38] Ataullah, I. Khan, S. Khattak, M. Shoaib, J. Kaewkhao, I. Ullah, G. Rooh, J. Alloys Compds. 875, 160095 (2021).
- [39] Ravina, Naveen, Sheetal, V. Kumar,
 S. Dahiya, N. Deopa, R. Punia, A.S. Rao,
 J. Lumin. 229, 117651 (2021).
- [40] G. Neelima, V.K. Kummara, N. Ravi, K. Suresh, S.N. Rasool, K. Tyagarajan, T.J. Prasad, *Mater. Res. Bull.* 110, 223 (2019).
- [41] S. Ghosh, J. Biswas, S. Jana, Phys. B Condens. Matter 699, 416819 (2025).
- [42] M.S. Sadeq, M.S. Al-Hammad, R. Al-Wafi, Ceram. Int. 50, 115 (2024).
- [43] G. Dedeepya, S. Mahamuda, K. Swapna, M. Venkateswarlu, A.S. Rao, Solid State Sci. 163, 07888 (2025).
- [44] A. Indhrapriyadarshini, K.A. Naseer, M.K.K. Poojha, I. Kebaili, K. Marimuthu, Spectrochim. Acta A Mol. Biomol. Spectrosc. 324, 124963 (2025).
- [45] B.A. Kumar, B. Sreenivas, P. Indira, A.K. Bhatnagar, P.H. Bindu, Opt. Mater. 163, 116978 (2025).
- [46] N. Luewarasirikul, S. Sarachai, N. Intachai, K. Kirdsiri, S. Kothan, H.J. Kim, J. Kaewkhao, *Radiat. Phys. Chem.* 224, 112064 (2024).
- [47] A.M.A. Mostafa, H.M. Zakaly, S.A. Al-Ghamdi, S.A. Issa, M. Al-Zaibani, R.M. Ramadan, E.F. El Agammy, Mater. Chem. Phys. 258, 123937 (2021).
- [48] S. Selvi, K. Marimuthu, G. Muralidharan, J. Non-Cryst. Solids 461, 35 (2017).
- [49] R. Praveena, V. Venkatramu, P. Babu, C.K. Jayasankar, Phys. B Condens. Matter 403, 3527 (2008).
- [50] R. Abdel-Hameed, N. Abourashed, A. Ashmawy, E. Ali, B. Huwaimel, M. Abdallah, A. Hydaya, E.H. Abdel-Gawad, M. Elsafi, Ann. Nucl. Energy 217, 111384 (2025).

- [51] N. Effendy, M.H.M. Zaid, K.A. Matori et al., *Prog. Nucl. Energy* 153, 104418 (2022).
- [52] S. Bhattacharya, H.D. Shashikala, *Phys. B Condens. Matter* 571, 76 (2019).
- [53] I. Saber, A. Talbi, K. Dahmani et al., Ceram. Int. 51, 7775 (2025).
- [54] B. Srinivas, B.S. Chary, A. Hameed, M.N. Chary, M. Shareefuddin, *Opt. Mater.* 109, 110329 (2020).
- [55] A.M.A. Mostafa, S.A.M. Issa, E.F. El Agammy, H.M.H. Zakaly, B.M. Alotaibi, F. Gharghar, *Radiat. Phys. Chem.* 206, 110766 (2023).
- [56] F. Gami, I. Guizani, M.A. Sebak, M.A.A. Alzara, H.G. Alharbi, H.Y. Amin, E.A. Elkelany, *Ceram. Int.* 51, 8747 (2025).
- [57] P. Janoš, J. Ederer, V. Pilařová, J. Henych, J. Tolasz, D. Milde, T. Opletal, Wear 362— 363, 114 (2016).
- [58] E.I. Kamitsos, M.A. Karakassides, G.D. Chryssikos, J. Phys. Chem. 91, 1073 (1987).
- [59] J. Krogh-Moe, J. Non-Cryst. Solids 1, 269 (1969).
- [60] L. Stoch, M. Środa, J. Mol. Struct. **511–512**, 77 (1999).
- [61] R.D. Husung, R.H. Doremus, *J. Mater. Res.* **5**, 2209 (1990).
- [62] H. Dunken, R.H. Doremus, J. Non-Cryst. Solids 92, 61 (1987).
- [63] F.L. Galeener, G. Lucovsky, J.C. Mikkelsen Jr., Phy. Rev. B 22, 3983 (1980).
- [64] M.M. Ismail, H.A. Abo-Mosallam, A.G. Darwish, Ceram. Int. 51, 25828 (2025).
- [65] S. Rada, P. Pascuta, M. Culea, V. Maties, M. Rada, M. Barlea, E. Culea, J. Mol. Struct. 924-926, 89 (2009).
- [66] M.S. Gaafar, S.Y. Marzouk, H. Mady, *Philos. Mag.* 89, 2213 (2009).
- [67] S.S. Owoeye, F.I. Jegede, S.G. Borisade, Mater. Chem. Phys. 248, 122915 (2020).
- [68] M.S. Gaafar, S.Y. Marzouk, I.S. Mahmoud, H.Y. Amin, M.A. Hassan, A. Samir, H.M. Elsaghier, *Phys. B Condens. Matter* 707, 417183 (2025).
- [69] M.A. Ouis, M.A. Marzouk, J. Lumin. 223, 117242 (2020).
- [70] R. Ciceo-Lucacel, I. Ardelean, J. Non-Cryst. Solids 353, 2020 (2007).
- [71] M. Rada, S. Rada, P. Pascuta, E. Culea, Spectrochim. Acta A Mol. Biomol. Spectrosc. 77, 832 (2010).

- [72] W.A. Pisarski, J. Pisarska, W. Ryba-Romanowski, J. Mol. Struct. 744-747, 515 (2005).
- [73] S. Kaur, P. Kaur, G.P. Singh, S. Kumar, D.P. Singh, Opt. Mater. 47, 276 (2015).
- [74] S. Mohan, S. Kaur, D.P. Singh, P. Kaur, Opt. Mater. 73, 223 (2017).
- [75] G.P. Singh, J. Singh, P. Kaur, S. Kaur, D. Arora, R. Kaur, D.P. Singh, J. Non-Cryst. Solids 546, 120268 (2020).
- [76] G.P. Singh, S. Kaur, P. Kaur, D.P. Singh, *Phys. B Condens. Matter* 407, 1250 (2012).
- [77] D. Singh, K. Singh, B.S. Bajwa, G.S. Mudahar, D.P. Singh, Manupriya, M. Arora, V. K. Dangwal, J. Appl. Phys. 104, 103515 (2008).
- [78] N.S. Prabhu, V. Hegde, M.I. Sayyed,
 O. Agar, S.D. Kamath, *Mater. Chem. Phys.* 230, 267 (2019).
- [79] I. Abdullahi, S. Hashim, S.K. Ghoshal, A.U. Ahmad, *Mater. Chem. Phys.* 247, 122862 (2020).
- [80] M.N.A. Hazlin, M.K. Halimah, F.D. Muhammad, J. Lumin. 196, 498 (2018).
- [81] W.T. Carnall, P.R. Fields, K. Rajnak, J. Chem. Phys. 49, 4424 (1968).
- [82] C.K. Jayasankar, P. Babu, J. Alloys Compds. **307**, 82 (2000).
- [83] R. Van Deun, K. Binnemans, C. Gorller-Walrand, J.L. Adam, *Proc. SPIE* 3622, 175 (1999).
- [84] S. Selvi, K. Marimuthu, G. Muralidharan, J. Lumin. 159, 207 (2015).
- [85] P. Kaur, S. Kaur, G.P. Singh, D.P. Singh, Solid State Commun. 171, 22 (2013).
- [86] S. Mohan, S. Kaur, P. Kaur, D.P. Singh, *J. Alloys Compds.* **763**, 486 (2018).
- [87] S. Kasap, H. Ruda, Y. Boucher, Cambridge Illustrated Handbook of Optoelectronics and Photonics, Cambridge University Press, New York 2009.
- [88] J. Tauc, A. Menth, J. Non-Cryst. Solids 8-10, 569 (1972).
- [89] Y. Zorenko, V. Gorbenko, T. Voznyak, T. Zorenko, Phys. Status Solidi b 245, 1618 (2008).
- [90] J. Zhang, D.L. Yang, E.Y.B. Pun, H. Gong,H. Lin, J. Appl. Phys. 107, 123111 (2010).
- [91] M.J. Lochhead, K.L. Bray, *Chem. Mater.* **7**, 572 (1995).
- [92] N. Bednarska-Adam, M. Kuwik, T. Goryczka, W.A. Pisarski, J. Pisarska, Opt. Mater. X 22, 100311 (2024).